

# Comprehensive Electromagnetic Transient Simulation of AC/DC Grid With Multiple Converter Topologies and Hybrid Modeling Schemes

ZHUOXUAN SHEN (Student Member, IEEE) AND VENKATA DINAHAHI (Senior Member, IEEE)

Department of Electrical and Computer Engineering, University of Alberta, Edmonton, AB T6G 2V4, Canada

CORRESPONDING AUTHOR: Z. SHEN (zshen@ualberta.ca)

This work was supported in part by the Natural Science and Engineering Research Council of Canada and in part by the China Scholarship Council.

**ABSTRACT** HVDC projects and renewable energy sources are increasingly being integrated into traditional AC grids, forming a more complex and yet sustainable power system. This paper focuses on the comprehensive electromagnetic transient (EMT) simulation of an AC/DC grid, which is composed of CIGRÉ dc grid test system, IEEE 39-bus AC system, and wind farms. The AC/DC converters are composed by different topologies of voltage source converters, including modular multilevel converters (MMCs), three-level neutral-point-clamped converters, and two-level converters. Piecewise polynomial curve fitting is proposed to the insulated gate bipolar transistor modules in the MMC. Furthermore, hybrid modeling schemes are proposed with different levels of complexity on the AC/DC grid to obtain accurate and efficient EMT simulation on PSCAD/EMTDC<sup>®</sup>. Three-zone partition schemes based on distance, node number, and network coupling are also proposed and compared. The performance of the proposed schemes is presented and verified with a DC fault case study.

**INDEX TERMS** Electromagnetic transient simulation, HVDC grid, hybrid modeling, insulated gate bipolar transistor (IGBT), modular multilevel converter (MMC), wind farm.

## I. INTRODUCTION

**H**VDC transmission has the advantage of low energy loss, low overall investment, greater controllability, high capacity long distance power transmission capability for the future power grid upgrading [1]–[7]. Many multi-terminal HVDC projects can be further connected either by DC/DC converters or AC systems creating a meshed DC grid. The DC transmission system offers an efficient solution to transfer the energy from the remote off-shore renewable sources to the conventional AC grid, which composes the modern AC/DC grid. The complexity of the large-scale AC/DC system makes the control and protection a significant challenge to ensure the steady-state and safe operation under different contingencies, such as DC and AC faults. Detailed electromagnetic transient simulation is necessary to study and analyze the transient phenomena of the AC/DC system [8]–[13].

This paper is focused on the efficient and accurate electromagnetic transient simulation of a complex AC/DC transmission system on PSCAD/EMTDC<sup>®</sup>. The proposed AC/DC grid integrates the CIGRÉ DC grid test system, IEEE 39-bus system, and wind farms, as shown in Fig. 1 [2], [14]. The DC grid is specifically focused on in this work, which employs various converter topologies including modular multilevel converter (MMC), 3-level neutral-point-clamped (3L-NPC) converter, 2-level (2L) converter, and four-quadrant DC/DC converter.

Among the different converter topologies, the MMC has the advantages of low switching frequency, low harmonics, and high modularity, which is also challenging for electromagnetic transient simulation due to the complex circuit topology [9], [15], [16]. Thévenin equivalence scheme is often used for MMC modeling to reduce the number of electrical nodes [17]. Instead of using the two-state resistor

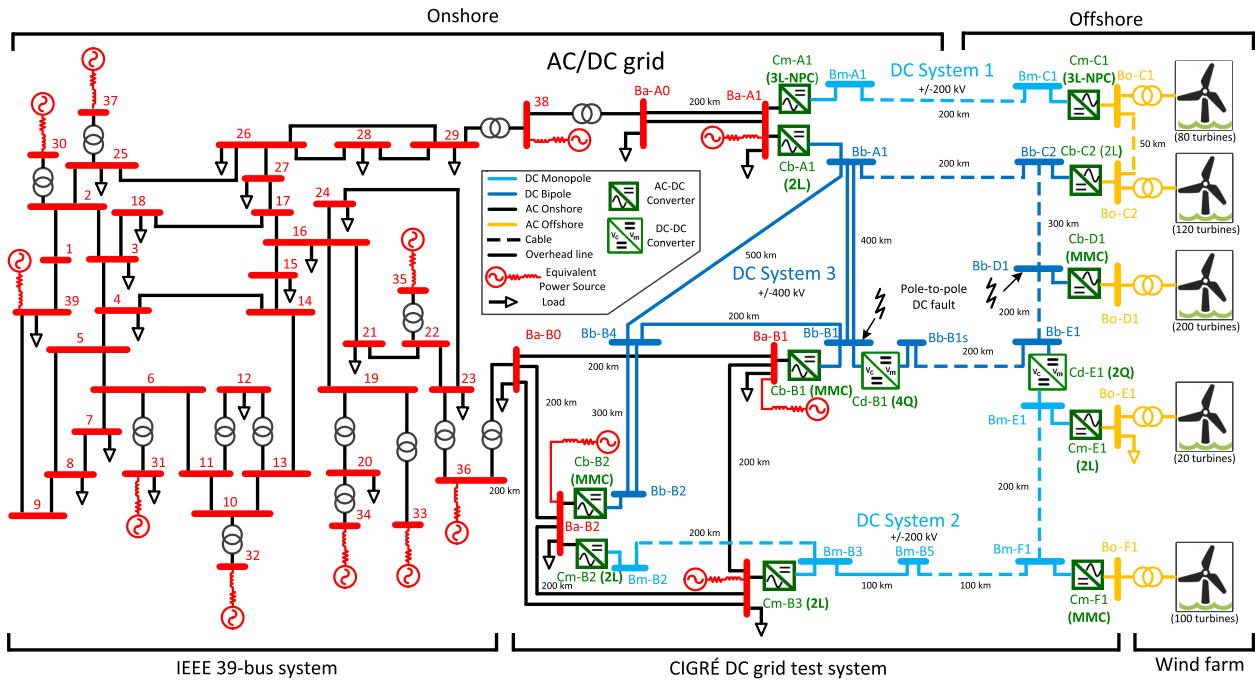


FIGURE 1. Topology of the AC/DC grid.

for IGBT module modeling, this work proposes the piecewise polynomial curve fitting modeling method for the IGBT module in the MMC sub-modules (SMs) to increase the simulation accuracy.

The computation effort for EMT simulation can increase significantly with the scale of the AC/DC grid. Model reduction or model equivalence is often adopted to decrease the calculation time for a large system. For instance, average value model and switching function model can be used to model AC/DC converters instead of using discrete switching devices [2], [18].

In this work, a *hybrid modeling scheme* is applied to the system, which is defined as utilizing multiple model complexities of the converters and other elements at different locations in the EMT-type simulation for the purpose of obtaining optimal performance of both accuracy and simulation speed. The most detailed model is used for the most interesting component or area. Two criteria of zone division are defined. The system can be partitioned into study zone and external zone based on the simulation purpose. The study zone contains the nodes and components where the transient event happens or detailed observation is required, and the external zone contains the rest of the components. The system can also be partitioned into a detailed zone, accurate zone, and averaged zone based on the model complexity. For a specific circuit and simulation purpose, the study zone is given, for instance, the fault location, the location of the controller and protection relay requiring parameter tuning. It can be challenging to determine the zones of different model complexity to achieve optimal performance of efficiency and accuracy.

This work proposes three zone partition schemes based on distance, node number, and network coupling with result comparison. The circuit topology reduction is not applied in this work to ensure the flexibility of changing the study zone. By changing the model complexity, the components at any location can be included in the study zone.

The major contribution of this work is the proposed MMC modeling method, the detailed electromagnetic simulation of the complex AC/DC grid, and the zone partition schemes using different converter model complexities. A matrix mapping scheme is proposed in this work to illustrate the zone partitioning. The paper is organized as follows: Section II presents the description of the AC/DC grid and the modeling schemes for various components; Section III discusses the zone partition schemes; Section IV presents the case studies and the simulation results, followed by the conclusions in Section V.

## II. AC/DC GRID DESCRIPTION AND HYBRID MODELING

As shown in Fig. 1, the AC/DC grid is composed of onshore IEEE 39-bus system, the offshore wind farms and the CIGRÉ DC grid test system, which emulates a modern transmission system efficiently integrating renewable energy sources. The CIGRÉ DC grid, which contains 3 DC transmission systems, was designed by CIGRÉ working groups as a common reference for DC grid study [2]. In the original report, MMCs are used for all the AC/DC converters with averaged model [2]. In this work, hybrid converter topologies, including MMC, 3L-NPC converter, and 2L converter, are adopted with the topologies shown in Fig. 2(a)-2(c), for the purpose of

presenting a more variant and realistic test scenario. Four-quadrant DC/DC converter is applied for Station Cd-B1 [Fig. 2(d)], while two-quadrant DC/DC converter is used for Station Cd-E1 [right side or left side of Fig. 2 (d)]. For

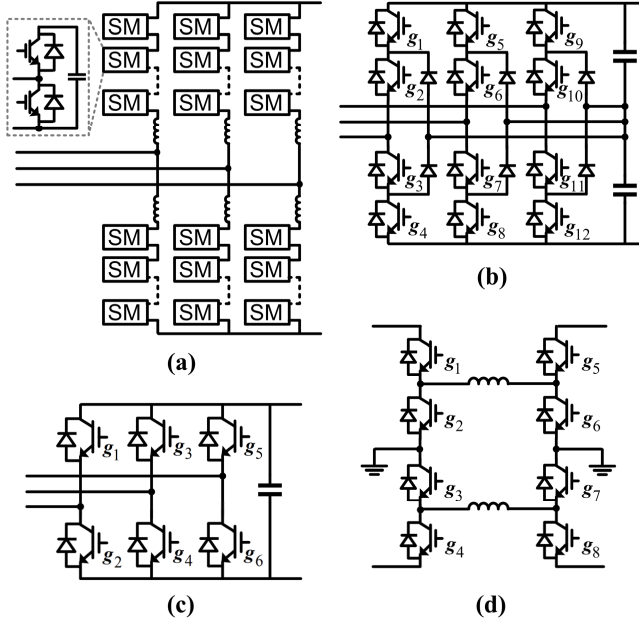


**FIGURE 2.** Topologies of converter: (a) modular multilevel converter, (b) three-level neutral-point-clamped converters, (c) two-level converter, and (d) four-quadrant DC/DC converter.

convenience, 60 Hz is used for all the AC transmission systems, although the AC system frequency connecting the wind farms can be different. The control diagram of the AC/DC converter is shown in Fig. 3, which is composed of outer loop control, inner current loop control, and the pulse width modulation (PWM) generator. The voltage droop control is added to regulate the DC voltage for power sharing. For MMC, phase disposition method is used for capacitor voltage balancing, which is equivalent as staircase modulation for high-level MMC [19].

The electromagnetic transient simulation is conducted for the proposed AC/DC grid with hybrid modeling complexity. Among various components, the converters, especially the MMCs, in the DC grid are specifically focused on for accurate modeling in this work. The proposed piecewise polynomial curve fitting method for MMC modeling is described in detail, while different types of models for converters and other elements are briefly reviewed.

### A. PROPOSED MODELING SCHEME FOR MMC

The topology and the circuit model of a half-bridge MMC SM are shown in Fig. 4(a) and 4(b). Each IGBT module, containing an IGBT and an anti-parallel connected diode, is modeled by series connected nonlinear resistor and voltage source representing the slope resistance  $r_{on}$  and the threshold voltage  $v_{on}$  in this work to increase the modeling accuracy compared with the two-state resistor model conventionally

applied for Thévenin equivalence based MMC model. The leakage resistance  $R_{leak}$  is added in parallel with the capacitor, modeled with series connected equivalent resistor  $R_c$  and history term  $v_c^{Hist}$ . Fig. 4(d) shows the output characteristics of the IGBT and diode from the manufacturer's datasheet [20].

This paper proposes the scheme of applying multiple polynomial functions to fit the highly nonlinear characteristics, as the following equations:

$$v(i) = \sum_{i=0}^n a_n i^n \quad (1)$$

$$r_{on} = \frac{dv}{di}, \quad v_{on} = v(i) - r_{on}i. \quad (2)$$

The entire  $v$ - $i$  curve is divided into three sections. Section I is the region where current is very small and grows exponentially with the increase of the voltage. The current in Section I has little impact on the system simulation and is normally not presented in the datasheet. Therefore a large constant resistance is used to model this region. Section II is modeled with a third order polynomial function for the nonlinear characteristics. Higher orders can obtain extra accuracy, however, with the cost of extra computation burden. When the current increases, the resistive relation dominates; therefore, Section III is modeled with a first-order equation. More sections can also be applied to improve the fitting accuracy and can ease the issue of discontinuity of the section boundaries. Since the SM current is the same in one arm, the additional calculation time for the nonlinear resistance and voltage sources is small and does not increase with the SM numbers. The fitted parameters of polynomial functions for the IGBT and diode characteristics and their corresponding fitting errors are listed in Table 1.

The exact resistances and voltage source values of the upper and lower IGBT modules ( $r_1$ ,  $v_1$ ,  $r_2$ , and  $v_2$ ) are determined based on the gating signals and the direction of the SM current  $i_{sm}$ . Thévenin equivalence is then applied for node elimination, given as follows:

$$v_{sm}(t) = r_{sm}i_{sm}(t) + v_{sm}^{Hist}(t - \Delta t) \quad (3)$$

where

$$r_{sm} = \frac{((R_c + R_{leak})r_1 + R_c R_{leak})r_2}{(R_c + R_{leak})(r_1 + r_2) + R_c R_{leak}} \quad \text{and} \quad (4)$$

$$v_{sm}^{Hist}(t - \Delta t) = \frac{(v_c^{Hist}(t - \Delta t) - v_1 - v_2)(R_{leak} + R_c)r_2}{(R_c + R_{leak})(r_1 + r_2) + R_c R_{leak}} + v_2. \quad (5)$$

Then the SM equivalent resistor  $r_{sm}$  and history term  $v_{sm}^{Hist}$  of the same arm are summed to form the interface for the system-level circuit. With the proposed model, the detailed waveforms of both the capacitors and individual IGBT modules can be presented accurately as well as the conduction power losses of switches. Because the datasheet only provides the current range of normal operation, the curve fitting may not be accurate if an extreme large current goes through the device. In this work, the proposed model is

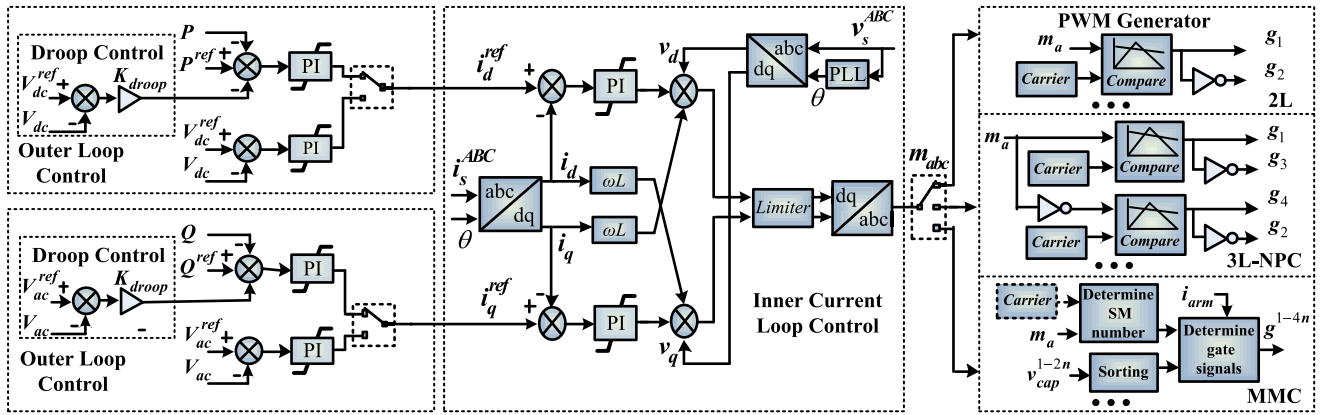


FIGURE 3. AC/DC converter control scheme.

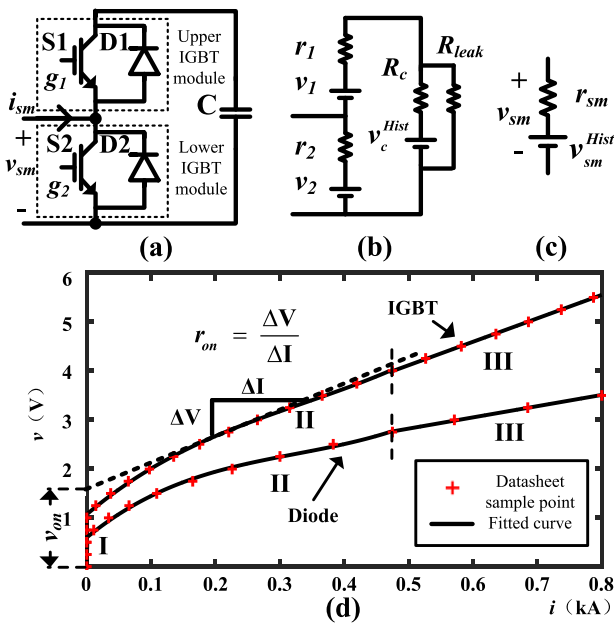


FIGURE 4. SM modeling scheme: (a) half-bridge structure, (b) circuit model, (c) Thévenin equivalence model, and (d) output and forward characteristics of IGBT and diode.

realized by designing user-defined module with Fortran code in PSCAD/EMTDC®.

**B. TWO-STATE RESISTOR MODEL**

The two-state resistor model uses a resistor with two distinct values to present the switching state, which are a small value for on-state and a large value for off-state. This model is a simple type of discrete switch model, while it cannot represent the detailed and accurate characteristics of IGBT modules.

**C. SWITCHING FUNCTION MODEL**

The switching function model uses the voltage sources at AC side and the current source at DC side, with the

waveforms controlled by the IGBT gate pulses, DC side voltage and AC currents. The circuit topology is similar for various converter types, except for the additional arm inductors in MMC. For the MMC, the switching function model can not be used to verify the capacitor voltage balancing algorithm, since the voltages are assumed to be the same. Since the value of the equivalent voltage source and the current source is based on the data of last time-step, errors and even oscillation may occur, which can also happen for the average value model.

**D. AVERAGE VALUE MODEL**

The average value model uses similar topology as the switching function model, except using the fundamental frequency waveform instead of switching function waveforms. For different converter topologies, the harmonics induced by switched waveform are ignored. Therefore, this model cannot effectively differentiate multiple converter topologies and can not be used to analyze the converter harmonics. For the MMC, especially with high levels, the system-level waveforms will not seem very different compared with the other detailed modeling schemes during steady-state operation. When using averaged model, the PWM control is not necessary and can be neglected, which saves the computation effort for controllers.

**E. WIND FARM**

The wind farm by itself can be a complex system, which may involve hundreds of generation units. The fixed-speed wind generator is used in this work, composed of the wind turbine, drive train, induction machine, pitch angle controller, compensating capacitor, and step-up transformer [14]. A controlled current source is connected in parallel with the single wind turbine modeled in detail, which has the value of n-1 (n is the number of the wind generators in a wind farm) times the current going through the single unit. In this way, the wind farm can be represented by the duplication of a single generation unit. If the wind farm is not the object of

**TABLE 1. Fitted parameters of polynomial functions for IGBT and diode characteristics.**

Device	Section II					Section III		
	$a_3$	$a_2$	$a_1$	$a_0$	error	$a_1$	$a_0$	error
IGBT	19.332	-19.501	11.118	1.069	1.50%	4.787	1.720	0.16%
Diode	25.950	-25.319	10.743	0.598	2.48%	2.292	1.675	0.36%

interest, it can be simplified to be a single induction machine or even an equivalent voltage source in series with impedance. Alternately, more detailed and complex wind turbine models, such as variable-speed wind generator based on doubly-fed induction machine and the corresponding converters, can also be included.

### F. TRANSMISSION LINE/CABLE AND OTHER ELEMENTS

The major transmission line and cable models include frequency dependent model, Bergeron model (traveling wave model), and PI section model (at fundamental frequency), etc. The first two types are distributed model, while the third one is a lumped model. The distributed model presents the delay property of traveling waves, which can be used to effectively and conveniently decompose the entire circuit topology into multiple sub-systems. The PI section model has a straightforward topology with few data input; however, it cannot decompose the system topology, and can consume longer computation time for a large system. For DC transmission line, high frequency harmonics induced by converter switching can be significant instead of the fundamental frequency of AC system. Therefore, the Bergeron model is not sufficient and accurate for DC transmission line system even under steady-state operation. The system also contains other elements, such as transformers, synchronous generators, etc. The AC system model can be made more complex by including the nonlinearities, such as the saturation and hysteresis of transformers.

The judgment of the accuracy and efficiency of a certain model is highly dependent on the application. The major focus of this work is the AC/DC converter modeling with multiple topologies and different modeling complexity. In this work, other elements are considered as control variables, and use fixed and feasible modeling schemes. Since this work adopts relatively simple topology of DC/DC converters, the DC/DC converters use discrete switches for modeling without further simplification. In the IEEE 39-bus system, the Bergeron model is used for AC transmission lines, since only the impedance of system frequency is provided, and the voltage source in series with impedance is used to represent the generators. Frequency dependent modeling is applied to the DC transmission lines and cables.

### III. GRID PARTITION SCHEMES

To optimize the accuracy and efficiency of the electromagnetic simulation of large AC/DC grid, the converter modeling of multiple complexities is applied for different zones. This

section describes three partition schemes based on distance, node number, and network coupling. In addition to the application in this work, the circuit partitioning schemes has wide applications, such as the hybrid simulation of transient stability and electromagnetic transient simulation, and node tearing for parallel calculation.

#### A. DISTANCE

The modeling scheme can be simpler if the distance is far from the center of the study zone, which can be a single node or multiple nodes. The scheme is based on the assumption that the longer distance of transmission lines can have larger impedance and need longer latencies for the traveling waves, and the components at remote locations can have minor and delayed effect on the electromagnetic transients. This scheme is straightforward, and has most clear and certain criteria for partitioning. It is particularly useful when the circuit topology is similar to the tree structure without forming loops at remote end as shown in Fig. 5(a), which is common for a distribution network. A case disobeying this scenario could be the

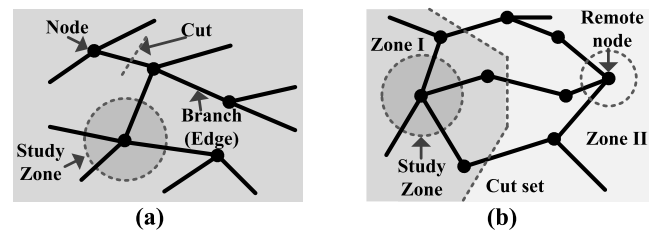


**FIGURE 5. Circuit topology: (a) tree structure and (b) mesh structure.**

existence of a remote electrical bus which has multiple paths connecting to the study zone as shown in Fig. 5(b), which is common in a transmission network. This remote bus will be partitioned into the accurate or averaged zone by the scheme based on distance; however, it has significant influence to the study zone. This drawback can also happen on the node number based scheme.

#### B. NODE NUMBER

The electrical nodes between the converter location and the center of study zone can be another significant indicator for zone partition. Simpler models can be used for the converters when the electrical node number is large. Actually, the node number shall refer to the one existing in the matrix equation instead of the circuit topology. The determination of exact node numbers can be challenging, which requires detailed

knowledge of modeling scheme and solution algorithm of a specific EMT software. The node elimination scheme for a certain element or a group of elements can be different for various programs. For simplicity and certainty, the electrical nodes in this work refer to the ones existing in the circuit topology, which are the AC and DC buses in the case study. A matrix mapping method is proposed to illustrate the concept of node number partitioning, which is similar to the procedure of constructing the conductance matrix. The diagonal element, which is a cross, stands for the circuit node or bus in the circuit topology. Whenever a connection exists between two nodes, crosses are symmetrically placed at the intersection of corresponding rows and columns of the two nodes. The dashed line, which must go through the off-diagonal cross, as shown in Fig. 6, is a connection between the two buses. The node number is the minimum off-diagonal crosses

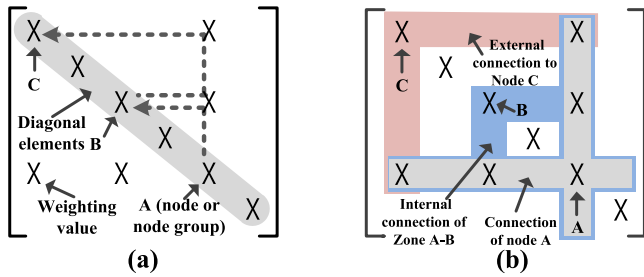


**FIGURE 6. Matrix mapping scheme: (a) node number illustration and (b) connection layer illustration.**

for all possible routes between two nodes. For example, the node number between Node A and Node B is 1, while the node number between Node B and Node C is 2. The node number can be determined from either the circuit topology or the proposed matrix mapping. The elements in a conductance matrix stand for the conductances connecting to a node, while the cross in the matrix mapping may represent a group of nodes or elements for the purpose of presenting the connectivity or coupling relation of a circuit topology. The off-diagonal elements can be later replaced by other meaningful values to represent the connectivity.

**C. NETWORK COUPLING**

Network coupling refers to the coupling strength between components or sub-networks. If multiple paths exist between two components, they are considered strongly coupled. In many cases, the coupling of the electromagnetic field is much weaker than direct galvanic connection. Galvanic isolation can be a criterion for zone partition. Especially under contingency conditions, the fault may have a significant impact on the area without galvanic isolation though far from the study zone. The nominal power flow and short circuit capacity is another factor. With large power flows between two networks, the coupling strength is considered strong. The partition process is to apply a cut set for the circuit topology. A weighting function can be applied for each branch, considering the above aspects, including galvanic

isolation, power flow, etc. In addition, the size of each zone can be applied as the constraint to determine the cut set. More future research work is needed to determine the appropriate weighting function and the corresponding coefficients. The process can also be interpreted as the matrix mapping scheme. As shown in the Fig. 6(b), The top layer, which covers the row and column of Node A, indicates the connections of Node A; the middle layer indicates the internal connections of the zone composed of Nodes A and B; the bottom layer indicates the external connections of Zone A-B. The weighting value can replace the off-diagonal crosses. Finding minimum total coupling strength is equivalent to finding the zone with the minimum sum of the weighting values located in the bottom layer. It is noted that the matrix mapping does not necessarily give a more intuitive solution than the circuit topology graph, while it offers a different perspective to observe the circuit.

In this work, the DC grid is composed of three DC systems. There are limited connections between the DC systems, and the DC/DC station does not provide galvanic isolation. Therefore the coupling between DC Systems 3 and 2 is deemed stronger than the coupling between DC Systems 3 and 1. This work uses the naturally existed partitioning of the three DC systems in the CIGRÉ DC grid, while the above-mentioned schemes can be developed for a more general circuit in future work.

**IV. CASE STUDIES AND SIMULATION RESULTS**

This section presents the simulation results of various tests and case studies, to verify the proposed MMC modeling scheme, compare the converter modeling of different complexities, and illustrate the hybrid modeling schemes, in the following three sub-sections, respectively. The CIGRÉ DC grid test system is used for the first two sub-sections, while, for the third sub-section, the complete AC/DC grid is utilized.

**A. VERIFICATION OF PROPOSED MMC MODELING SCHEME**

Fig. 7 compares the simulation results between the proposed piecewise polynomial curve fitting scheme and the two-state resistor model for MMC. Pole-to-pole DC fault with the fault resistance of 0.1Ω occurs at the DC bus Bd-D1 from 1.2s lasting for 0.05s, and the MMC Station Cb-D1 is chosen for observation. Except for the difference of MMC modeling schemes, the remainder converter topologies all use discrete switches. It is observed that the differences of capacitor voltages and AC currents of the two models are significant at the beginning of the fault and then become smaller after few hundreds of milliseconds, as shown in Fig. 7 (a) and (b). The differences of DC current and DC voltage are much smaller compared with capacitor voltages. In other words, the steady-state results are very close to each other for the two models, while the transient waveforms can be different. This is due to the difference of IGBT module parameters, including the slope resistance and threshold voltage. The two-state resistor model does not consider the threshold voltage and uses idealized resistances for IGBT modules, which are

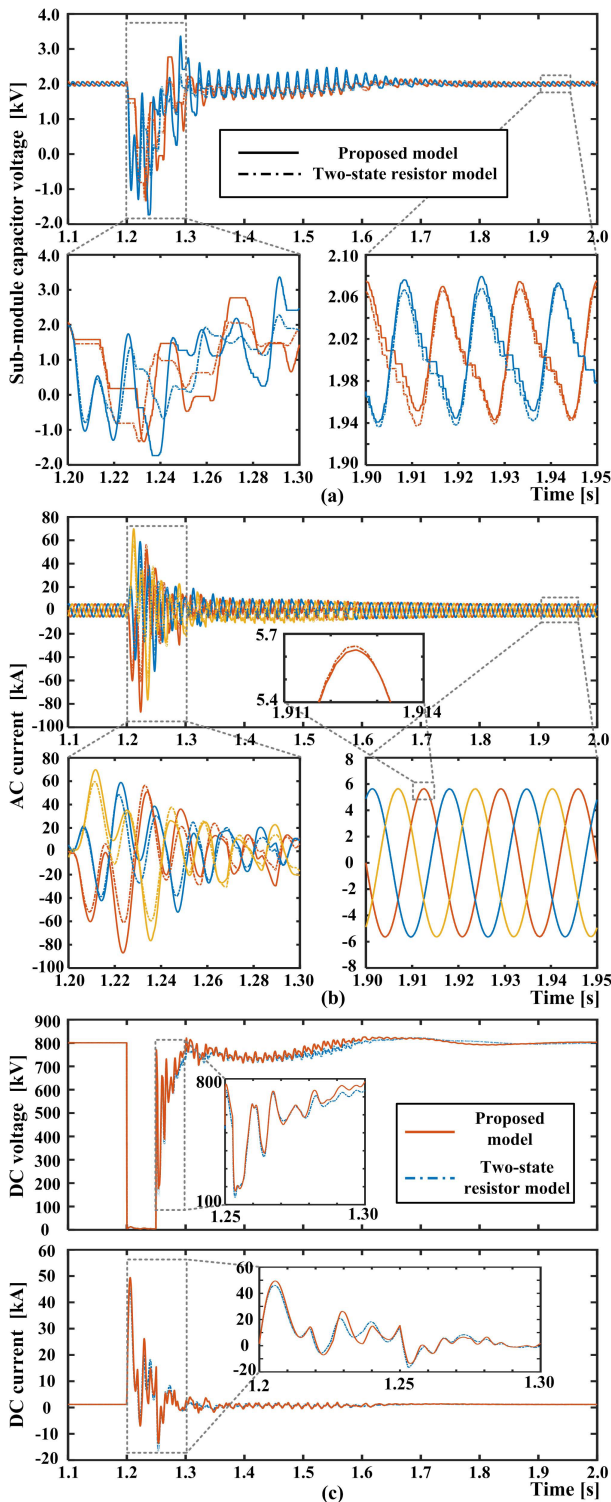


**FIGURE 7.** Comparative results between the proposed model and the two-state resistor model of MMC at Station Cb-D1: (a) capacitor voltages of the first SM in the upper and lower arms of phase-a, (b) AC current, and (c) DC voltage and DC current.

very large value for turn-off state and very small value for turn-on state. In contrast, the proposed model uses accurate curve fitting for the IGBT and diode characteristics from the manufacturer's datasheet. When the DC fault occurs, the current can be multiples of the steady-state value, which

makes the IGBT module characteristics more significant for simulation accuracy. The parameter influence is larger for the waveforms of a single device or sub-module, compared with converter-level or system-level waveforms.

Both models have sufficient accuracy for system-level study and can monitor the sub-module capacitor voltage, while the proposed model can provide switching device level waveforms, such as the conduction losses, dynamically changing  $r_{on}$  and  $v_{on}$  for the IGBT modules as shown in Fig. 8. The power losses during the fault transient and steady-

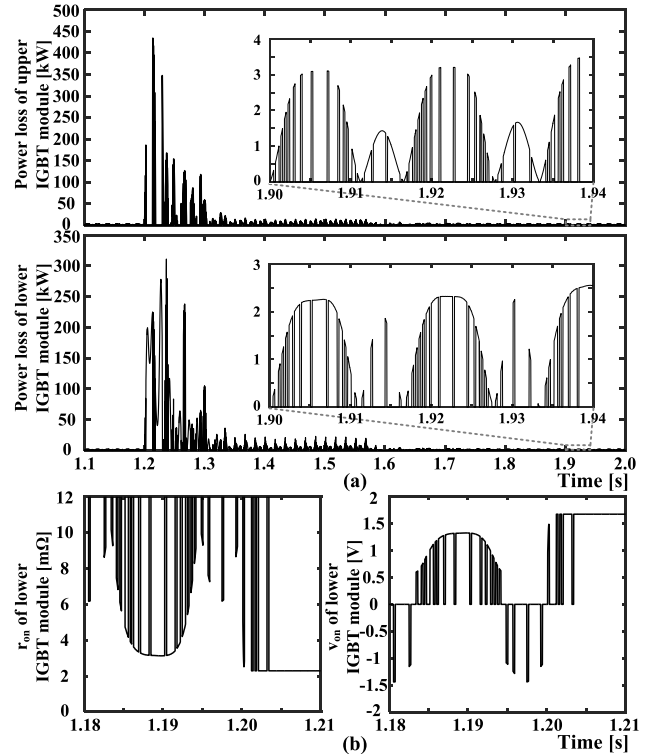


**FIGURE 8.** Switching device level waveforms in the first sub-module of upper arm of phase-a: (a) power losses of upper and lower IGBT modules and (b)  $r_{on}$  and  $v_{on}$  of lower IGBT module.

state are presented. During the fault, the instantaneous power losses can reach up to around 450 kW, which may damage the devices. Note that the performance of the protection devices, such as breakers, by-pass switches, are not included in the simulation, which can limit the over current and protect the devices effectively. Fig. 8(b) shows the dynamic change of  $r_{on}$  and  $v_{on}$  according to the gate pulses and the SM current. When the IGBT module is turned off, the resistor value is  $1\text{M}\Omega$ , which can not fit in Fig. 8(b). When the fault happens, the current is located in Section III of Fig. 4(d), which makes the  $r_{on}$  and  $v_{on}$  unchanged for the corresponding period.

## B. COMPARISON OF VARIOUS CONVERTER MODELING COMPLEXITIES

In this sub-section, the proposed model (discrete switches applied for 2L and 3L-NPC converter modeling), two-state resistor model (discrete switches applied for 2L and 3L-NPC

converter modeling), switching function model, and average value model are used for the converters in CIGRÉ DC grid test system. The test condition is the same as in the previous sub-section, which is the pole-to-pole DC fault at Bus Bb-D1 from 1.2s. The comparison of results of DC voltage and DC current at multiple converter stations are presented in Fig. 9, and the following phenomena can be observed.

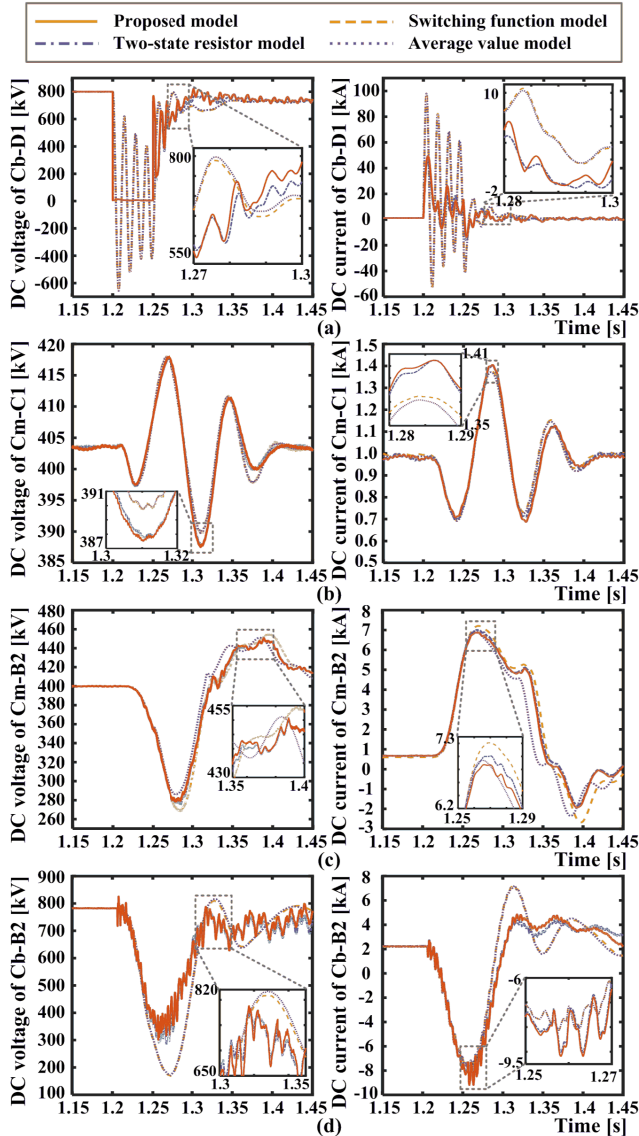


**FIGURE 9.** Comparative results of using different model complexities: (a) DC voltage and DC current at Station Cb-D1, (b) DC voltage and DC current at Station Cm-C1, (c) DC voltage and DC current at Station Cm-B2, and (d) DC voltage and DC current at Station Cb-B2.

1) At Station Cb-D1, which is the DC fault location, both the DC voltage and current waveforms using switching function model and average value model have severe numerical oscillations, which leads to the spurious results. After few hundred milliseconds, oscillations subside and the waveforms

reach steady-state. This happens mainly because the model interface uses delayed voltage and current information, which can cause the numerical issues when abrupt change occurs. Applying iterations between the AC and DC side may solve the issue; however, this is not supported by PSCAD/EMTDC®, and can consume longer calculation time.

- 2) At the station far away from the fault location, the switching function model and the average value model do not have numerical issues. However, the error is relatively large compared with more detailed models.
- 3) For the MMC modeling, SM capacitor balancing is not considered for the switching function model and the average value model, which can have a significant impact on the transient behavior and lead to a larger error during transients compared with the scenarios for 2L and 3L-NPC converters. Since the voltages of MMC with high levels are almost perfect sinusoidal waveforms, therefore the system-level waveforms of the switching function model and average value model are almost identical. For 2L and 3L-NPC converters, the waveforms can be quite different for the switching function model and average value model, especially at the AC side of the converters.
- 4) Among the Stations of Cm-C1, Cm-B2, and Cb-B2, Station Cm-B2 has the largest disturbances, which is located in the same DC System 2 of the fault location, while Station Cm-C1 has the smallest disturbance, located in the DC System 1 which has the weakest coupling with DC System 2. This observation is consistent with the network coupling discussion in Section III.

In summary, the switching function model and the average value model can be used in stations far away from the fault location with certain accuracy; however, they are not appropriate for use exactly at the fault location. Table 2 presents the execution time for a 5s run using different modeling schemes.

**TABLE 2.** Execution time comparison of CIGRÉ DC grid test system.

Model	Execution time (for a 5s run)
Proposed model	501s
Two-state resistor model	423s
Switching function model	119s
Average value model	107s

The simulation is conducted on the PC using Intel® Xeon CPU E5-2609 at 2.4GHz, 32 GB RAM, and Window 7 operating system. The additional execution time of the proposed method is small (while providing greater details) compared with the one using two-state resistor model, and the execution times of switching function model and average value model are close to each other and are much smaller compared with the Thévenin equivalence based methods.

**TABLE 3. Modeling scheme, converter station allocation, and execution time for the AC/DC grid case study.**

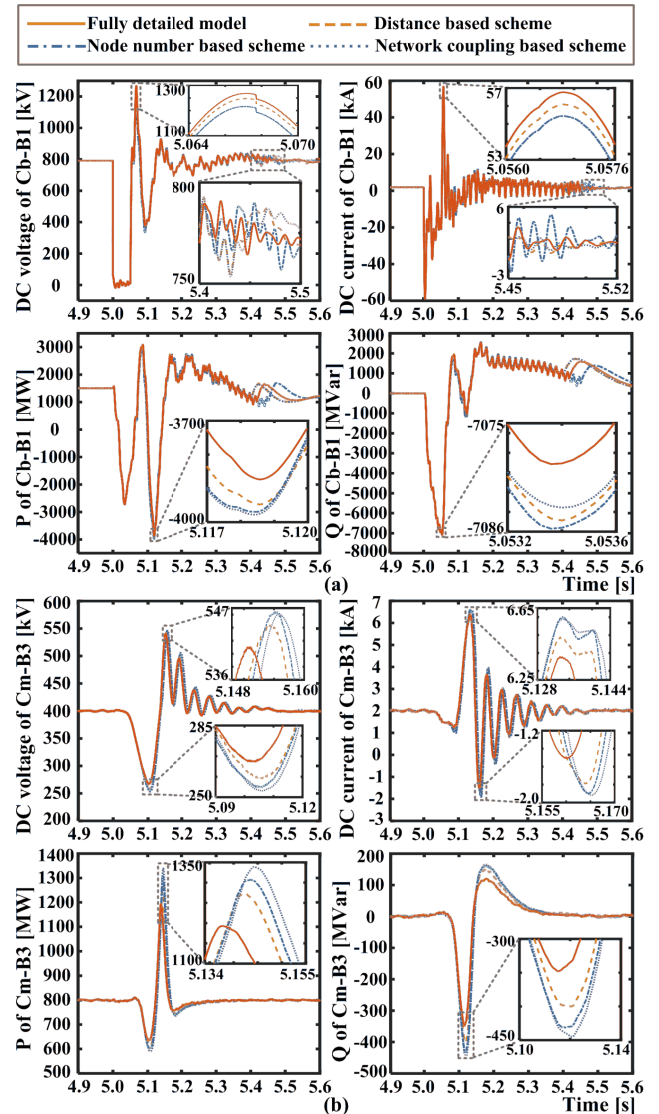
Converter/Partition scheme	Modeling method/Converter station allocation			Execution time (for a 5s run)
	Detailed zone	Accurate zone	Averaged zone	
MMC	Proposed model	Two-state resistor model	Average value model	NA
2L & 3L-NPC	Discrete switches	Switching function model	Average value model	NA
Full detailed model	All Stations	None	None	738s
Distance based scheme	Cb-B1,Cm-E1,Cm-B3	Cm-F1,Cm-A1,Cb-B2, Cm-B2,Cb-D1,Cb-A1	Cm-C1,Cb-C2	499s
Node number based scheme	Cb-B1,Cb-A1	Cb-B2, Cm-B3, Cb-C2, Cm-A1	Cm-B2,Cm-F1,Cm-E1, Cb-D1,Cm-C1	445s
Network coupling based scheme	Cb-B1	Cb-A1,Cb-C2, Cb-D1,Cb-B2	Cm-b2,Cm-B3,Cm-F1, Cm-E1, Cm-A1, Cm-C1	432s

### C. CASE STUDY OF HYBRID MODELING SCHEME

In this section, the complete AC/DC grid is used for the case study including the wind farms and IEEE 39-bus AC system. The DC fault lasting 0.05s from 5s of the simulation occurs at the DC Bus Bb-B1, which is close to the center of the test system. In the case study, the fault location and the converter stations around it are assumed as the study zone. Three zone partition schemes are applied based on distance, node number, and network coupling to divide the complete system into the detailed zone, accurate zone, and averaged zone. The modeling schemes for different zones are shown in the upper part of Table 3. Since the switching function model and the average value model have almost identical accuracy for MMC modeling, the two-state resistor model is applied for the accurate zone to differentiate it from the averaged zone.

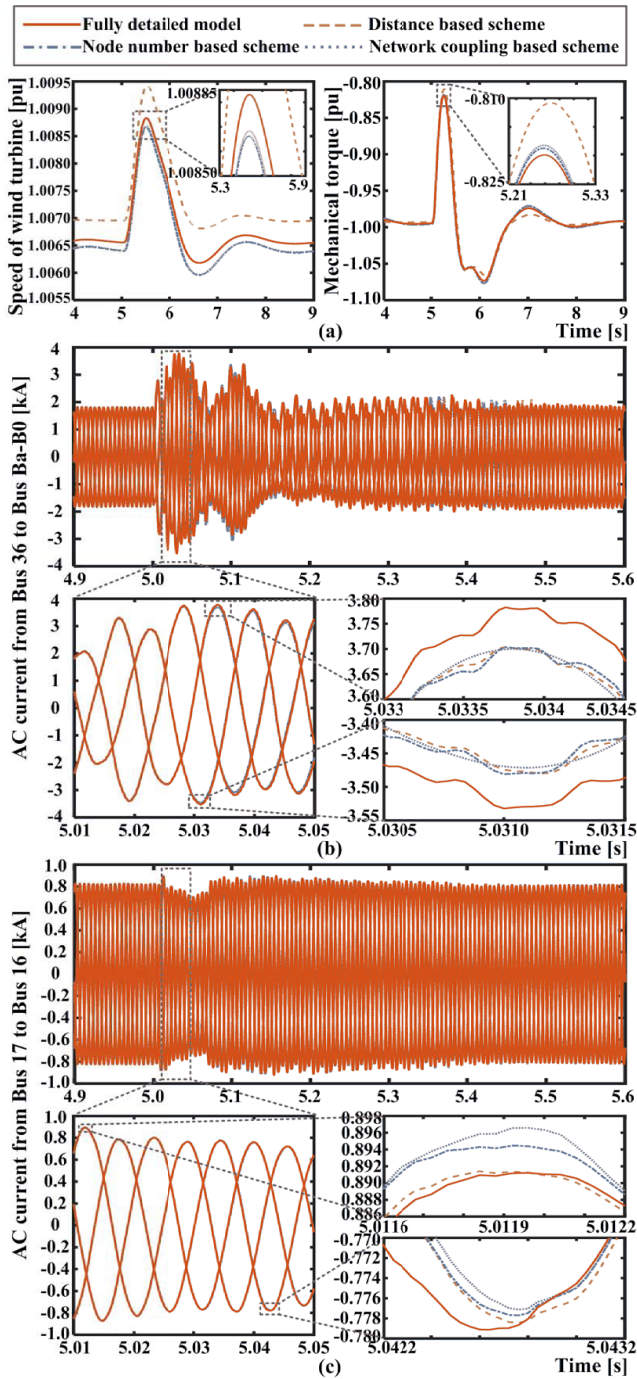
For distance based scheme, the detailed zone contains the converters within 300km, while the accurate zone contains the ones within 500km. For node number based partitioning scheme, the detailed zone contains the converters with the node number of 1 or 0 to the node of fault location, the accurate zone contains the converters that have the node number of 2 to the node of fault location. For the network coupling based scheme, the detailed zone only contains the Station Cb-B1, while all the Stations in DC system 3 are in accurate zone. The rest converters in corresponding schemes are located in averaged zone. The lower part of Table 3 presents the allocations of converter stations in the three zones for different partition schemes.

Fig. 10 and Fig. 11 present comparative results of converter stations, wind farm and AC system using different zone partition schemes as well as the case using all detailed models. By using the hybrid modeling scheme, the simulation accuracy is maintained for the transient analysis, though a certain amount of error exists. For Station Cb-B1, since all the schemes use the detailed model, the results using different partition schemes are quite consistent with each other, especially at the beginning of the transients. However, the waveforms notably differ from each other after around 400 milliseconds of the fault. This is because the converters using simplified modeling schemes are generally far from the fault location. The traveling wave latency of transmission lines delays the waveform discrepancy. When the



**FIGURE 10. Comparative results of converter stations using different partition schemes: (a) DC voltage, DC current, AC-side active power, and reactive power at Station Cb-B1, and (b) DC voltage, DC current, AC-side active power, and reactive power at Station Cm-B3.**

steady-state is reached, the waveforms become consistent eventually. The errors for different schemes are relatively large at Station Cb-B1 at the beginning of the transients due to



**FIGURE 11.** Comparative results of wind farms and AC systems using different partition schemes: (a) shaft speed and mechanical torque of the wind turbine connecting to Station Cb-D1, (b) AC current form Bus 36 to Bus Ba-B0, and (c) AC current form Bus 17 to Bus 16.

the modeling difference at the Station Cb-B1 and other nearby stations. Although the partitioning is based on different criteria, the zones overlap with each other to some extent. The similarity of AC/DC grid modeling between the fully detailed model case and other cases using hybrid modeling is not as much as the similarity among the different partition schemes, which is presented in Table 3. It explains the phenomenon

that the waveforms of detailed model is slightly different from the waveforms of the cases using hybrid modeling, while the waveforms between different partition schemes are close to each other, which can be observed, especially in Fig. 10(b) and Fig. 11(b). In Fig. 11(a), the shaft speed and the mechanical torque of the case using node number based scheme have notable error compared with other cases. Because the MMC Station Cb-D1 uses average value model for node number case, while other cases use at least the two-state resistor model. The control dynamics can affect simulation accuracy, which is neglected in the case using node number based scheme. In the on-shore AC system, it is clearly observed that the disturbance is much smaller for the location far away from the fault location.

If another location different from the fault location is desired, the partition schemes can be applied independently, which is equivalent to applying the superposition theorem. The modeling method of a certain station adopts the most detailed one, if the two partition results are not consistent.

The execution time of a 5s run is listed in Table 3. Using hybrid modeling schemes can reduce around 40% of the execution time compared with the case using fully detailed model. The speed-up can be more significant for a larger system, where the averaged zone can cover more converters. Although the case using distance based scheme consumes longer computation time, the case using node number based scheme obtains higher accuracy except for the waveform at the wind turbine connecting to Station Cb-D1 in Fig. 10 and Fig. 11. However, it is difficult to generally evaluate the performance of the three partition schemes, since it is affected by the circuit topology and simulation purpose.

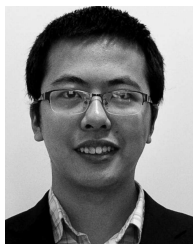
## V. CONCLUSION

The paper proposed the piecewise polynomial curve fitting scheme for MMC modeling, and presented the simulation results of a complete AC/DC grid using fully detailed model and hybrid modeling schemes. The hybrid modeling scheme can effectively balance the accuracy and the simulation speed. Although this work used PSCAD/EMTDC<sup>®</sup> as the implementation platform, the proposed model and the simulation of the AC/DC grid can be accomplished in other EMT tools, such as EMTP-RV<sup>®</sup>. The purpose of this work is to provide comprehensive electromagnetic modeling schemes and guidelines to develop the complex AC/DC grid system. Insights and accelerate gained through such simulation can greatly enhance the control and protection studies of the AC/DC grid system in future research.

## REFERENCES

- [1] D. van Hertem, O. Gomis-Bellmunt, and J. Liang, *HVDC Grids for Offshore and Supergrid of the Future*. Hoboken, NJ, USA: Wiley, 2016.
- [2] T. K. Vrana, Y. Yang, D. Jovicic, S. Denetiere, J. Jardini, and H. Saad. (2014). "The CIGRÉ B4 DC grid test system," Cigré, Paris, France, Tech. Rep. V15. [Online]. Available: <http://b4.cigre.org/Publications/Documents-related-to-the-development-of-HVDC-Grids>
- [3] X. Chen *et al.*, "Integrating wind farm to the grid using hybrid multiterminal HVDC technology," *IEEE Trans. Ind. Appl.*, vol. 47, no. 2, pp. 965–972, Apr. 2011.

- [4] A. A. Gebreel and L. Xu, "DC/AC power conversion based on using modular multilevel converter with arm energy approximation control," *IEEE Power Energy Technol. Syst. J.*, vol. 3, no. 2, pp. 32–42, Jun. 2016.
- [5] B. Wu, *High-Power Converters and AC Drives*. Hoboken, NJ, USA: Wiley, 2006.
- [6] S. Elimban, Y. Zhang, and J. C. G. Alonso, "Real time simulation for HVDC grids with modular multi-level converters," in *Proc. 11th IET Int. Conf. AC DC Power Transmiss.*, Birmingham, U.K., 2015, pp. 1–8.
- [7] K. Rouzbehi, J. I. Candela, A. Luna, G. B. Gharehpetian, and P. Rodriguez, "Flexible control of power flow in multiterminal DC grids using DC-DC converter," *IEEE J. Emerg. Sel. Topics Power Electron.*, vol. 4, no. 3, pp. 1135–1144, Sep. 2016.
- [8] H. W. Dommel, *EMTP Theory Book*. Portland, OR, USA: Bonneville Power Admin., 1984.
- [9] Z. Shen and V. Dinavahi, "Real-time device-level transient electrothermal model for modular multilevel converter on FPGA," *IEEE Trans. Power Electron.*, vol. 31, no. 9, pp. 6155–6168, Sep. 2016.
- [10] Y. Chen and V. Dinavahi, "Hardware emulation building blocks for real-time simulation of large-scale power grids," *IEEE Trans. Ind. Informat.*, vol. 10, no. 1, pp. 373–381, Feb. 2014.
- [11] G. G. Parma and V. Dinavahi, "Real-time digital hardware simulation of power electronics and drives," *IEEE Trans. Power Del.*, vol. 22, no. 2, pp. 1235–1246, Apr. 2007.
- [12] M. D. O. Faruque *et al.*, "Real-time simulation technologies for power systems design, testing, and analysis," *IEEE Power Energy Technol. Syst. J.*, vol. 2, no. 2, pp. 63–73, Jun. 2015.
- [13] X. Guillaud *et al.*, "Applications of real-time simulation technologies in power and energy systems," *IEEE Power Energy Technol. Syst. J.*, vol. 2, no. 3, pp. 103–115, Sep. 2015.
- [14] M. Singh and S. Santoso, "Dynamic models for wind turbines and wind power plants," Nat. Renew. Energy Lab., Golden, CO, USA, Tech. Rep. NREL/SR-5500-52780, 2011.
- [15] A. Lesnicar and R. Marquardt, "An innovative modular multilevel converter topology suitable for a wide power range," in *Proc. IEEE Bologna Power Tech Conf.*, Jun. 2003, vol. 3, p. 6.
- [16] S. Debnath, J. Qin, B. Bahrani, M. Saeedifard, and P. Barbosa, "Operation, control, and applications of the modular multilevel converter: A review," *IEEE Trans. Power Electron.*, vol. 30, no. 1, pp. 37–53, Jan. 2015.
- [17] U. N. Gnanarathna, A. M. Gole, and R. P. Jayasinghe, "Efficient modeling of modular multilevel HVDC converters (MMC) on electromagnetic transient simulation programs," *IEEE Trans. Power Del.*, vol. 26, no. 1, pp. 316–324, Jan. 2011.
- [18] J. Peralta, H. Saad, S. Denneriere, J. Mahseredjian, and S. Nguefeu, "Detailed and averaged models for a 401-level MMC HVDC system," *IEEE Trans. Power Del.*, vol. 27, no. 3, pp. 1501–1508, Jul. 2012.
- [19] M. Saeedifard and R. Iravani, "Dynamic performance of a modular multilevel back-to-back HVDC system," *IEEE Trans. Power Del.*, vol. 25, no. 4, pp. 2903–2912, Oct. 2010.
- [20] (2015). *Technical information, Infineon IGBT modules FZ400R33KL2C B5*. [Online]. Available: [https://www.infineon.com/dgdl/Infineon-FZ400R33KL2C\\_B5-DS-v02\\_00-en\\_de.pdf?fileId=db3a304412b407950112b4319b8554c4](https://www.infineon.com/dgdl/Infineon-FZ400R33KL2C_B5-DS-v02_00-en_de.pdf?fileId=db3a304412b407950112b4319b8554c4), Accessed on: Oct. 2013.



**ZHUOXUAN SHEN** (S'14) received the B.Eng. degree in electrical engineering from Jiangsu University, Zhenjiang, China, in 2013, and is currently working toward the Ph.D. degree in electrical and computer engineering at the University of Alberta, Edmonton, AB, Canada. His research interests include real-time simulation of power systems, power electronics, and field-programmable gate arrays.



**VENKATA DINAVAH** (S'95–M'00–SM'08) received the Ph.D. degree from the University of Toronto, Canada, in 2000. He is currently a Professor in electrical and computer engineering with the University of Alberta, Edmonton, AB, Canada. His research interests include real-time simulation of power systems and power electronic systems, large-scale system simulation, and parallel and distributed computing.